Journal of the Taiwan Institute of Chemical Engineers 000 (2017) 1–9

Contents lists available at ScienceDirect

Journal of the Taiwan Institute of Chemical Engineers

journal homepage: www.elsevier.com/locate/jtice

Nanoporous activated carbon prepared from karanj (*Pongamia pinnata*) fruit hulls for methylene blue adsorption

Md. Azharul Islam[a,b], S. Sabar[c], A. Benhouria[d], W.A. Khanday[a], M. Asif[e], B.H. Hameed[a,*]

[a] School of Chemical Engineering, Universiti Sains Malaysia, Engineering Campus, 14300 Nibong Tebal, Penang, Malaysia
[b] Forestry and Wood Technology Discipline, Khulna University, Khulna 9208, Bangladesh
[c] Chemistry Section, School of Distance Education, Universiti Sains Malaysia, 11800 Minden, Penang, Malaysia
[d] Laboratoire de Génie des Procédés Chimiques (LGPC), Faculté de Technologie, Université Ferhat Abbas Sétif-1, 19000 Sétif, Algerie
[e] Chemical Engineering Department, College of Engineering, King Saud University, P.O. Box 800, Riyadh 11421, Saudi Arabia

ARTICLE INFO

Article history:
Received 24 April 2016
Revised 1 January 2017
Accepted 20 January 2017
Available online xxx

Keywords:
Activated carbon
Adsorption
Dye
KOH activation
Karanj

ABSTRACT

In this study, karanj (*Pongamia pinnata*) fruit hulls were used as a precursor to prepare low-cost activated carbon with a large surface area through KOH activation. The prepared activated carbon (KFHAC) was characterized through pore structural analysis, scanning electron microscopy, and Fourier transform infrared spectroscopy. KFHAC presents a BET surface area of 828.30 m^2/g, a micropore volume of 0.36 cm^3/g, and an average pore size of 19.92 Å The adsorption performance of KFHAC was evaluated using methylene blue (MB) as the model adsorbate. Adsorption experiments indicated that the pseudo-second-order kinetic and Langmuir adsorption isotherm models can accurately describe the adsorption process. The maximum adsorption capacities (q_m) of MB were 154.8, 203.4, and 239.4 mg/g at 30 °C, 40 °C, and 50 °C, respectively. This study indicates that karanj fruit hull is a promising precursor for the production of low-cost and efficient activated carbon with a large surface area.

1. Introduction

Dye-containing effluents discharged by textile, paint, paper, plastic, cosmetic, and food processing industries have become a major concern. These industries produce more than 700 000 tons of dyes yearly, of which 50% is absorbed in surface waters [1]. Accumulation of untreated dyes in water sources may result in adverse effects to human health and the environment because these dyes exhibit a complex molecular structure with variable toxicity, carcinogenic, mutagenic, and allergenic properties. As untreated dyes are highly active and stable toward chemical, photochemical, and biological degradation, adsorption has emerged as a practical and effective technique to produce high-quality dye effluents.

Different types of fibrous adsorbents like chitosan [2,3] and polypropylene [4] have been developed in recent years for the adsorption of dyes. Activated carbon is a common and efficient adsorbent used to remove dyes from wastewaters because of its large surface area, high adsorption capacity, and diverse functional groups [5]. Nevertheless, large-scale application of activated carbon is hindered because this material is non-renewable and requires expensive precursors [6]. Thus, production of activated carbon from cheap and renewable precursors has been an interesting research subject. Lignocellulosic biomasses, such as *Albizia lebbeck* seed pod [6], rattan sawdust [7], rice husks [8], waste tea [9], biodiesel industry solid reside [10], cotton stalk [11], durian shell [12], oil palm ash [13], Iranian milk vetch [14], Soy meal hull [15], olive stone [16], rambutan peel [17], macadamia nut endocarp [18], peach stone [19], coffee ground [20], *Posidonia oceanica* fiber [21] and apricot stones [22], have been explored as possible precursors for the production of activated carbon.

Karanj (*Pongamia pinnata*) or Karanja is an evergreen, drought-resistant, nitrogen-fixing tree that belongs to the Leguminaceae family [23]. This fast-growing tree is commonly found in tropical and sub-tropical countries, such as Malaysia, India, Thailand, Vietnam, Philippines, China, Japan, Australia, New Zealand, and USA. Karanj is famous for its seeds, which contain 25–50 wt% of oil [24]. The seeds, which are kidney shaped and brownish red, can be easily collected from the fruits by using a hammer. The fruits are naturally flat and elliptic, with a length of 7.5 cm [25]. Each fruit contains one to two seeds, and a single tree can produce 9–90 kg of seeds with 25–40 wt% of oil [24]. With these properties, karanj has been recognized as an invaluable non-edible source of bio-oil for medical purposes and as a new feedstock for biodiesel production. As the demand for karanj bio-oil is predicted to increase in the near future, residual waste generated from oil extraction remains a major problem. During seed collection, large amounts of karanj

* Corresponding author.
E-mail address: chbassim@usm.my (B.H. Hameed).

http://dx.doi.org/10.1016/j.jtice.2017.01.016
1876-1070/

fruit hulls are disposed because they have no commercial value. In this regard, karanj fruit hulls can be used as a precursor to prepare activated carbon because this raw material is cheap, abundant, renewable and environment friendly.

The properties of activated carbon depend on the preparation method and the type of precursor. Activated carbon can be prepared through two basic methods: physical and chemical activation. Physical activation involves a step-by-step process, which requires the precursor to be first converted into carbonized material (char) and then activated by using an oxidizing gaseous agent, such as carbon dioxide, water vapor, or their mixture. Meanwhile, in chemical activation, the precursor is impregnated with activators and carbonized at different temperatures. In this technique, carbonization and activation are simultaneously performed, resulting in both physical and chemical modifications [17]. This method is also inexpensive and energy saving because low activation temperatures are required to produce high-yield and improved porous carbon structures. As a chemical activator, potassium hydroxide (KOH) is widely used to obtain porous carbons with high specific surface area and well-developed micropores [11].

This study aims to prepare a novel low-cost activated carbon with a large surface area from karanj fruit hulls (known as KFHAC) through KOH activation. The prepared adsorbent was characterized through pore structural analysis, scanning electron microscopy (SEM), and Fourier transform infrared (FTIR) spectroscopy. Adsorption kinetics, isotherms, and thermodynamics was outlined using methylene blue (MB) as the model adsorbate.

2. Materials and methods

2.1. Chemicals

MB (molecular weight: 373.9 g/mol, solubility in water: 40 g/l) was obtained from Sigma-Aldrich and used as adsorbate. All other chemicals, such as KOH and HCl, were of laboratory grade and purchased from different renowned suppliers.

2.2. Preparation of activated carbon

Karanj fruits were collected from the Engineering Campus, Universiti Sains Malaysia. The matured fruits were manually separated from the seeds by using a wooden hammer. Seed-free karanj fruit hulls (KFH-R) were washed and rinsed with deionized water to eliminate adherents. KFH-R was air dried for 3 days and then oven dried at 105 °C until a constant weight. After drying, the samples were crushed and sieved into a uniform size, ranging from 1 mm to 2 mm. Activated carbon was prepared through carbonization and activation by using previously reported methods [26]. Dried KFH-R and crushed raw materials were placed in a stainless steel vertical tubular reactor and carbonized in a tubular furnace at 600 °C with a heating rate of 10 °C/min for 1 h N_2 gas (99.995%) was simultaneously supplied to the system at a flow rate of 150 cm^3/min. After carbonization, the samples were cooled at room temperature under N_2 flow. The KOH solution was then mixed with the produced char at an impregnation ratio of 1:3 (w/w%) for 24 h and dehydrated overnight in an oven at 105 °C. The samples were activated under conditions similar to that used in carbonization. After cooling at room temperature, the activated products were washed with 0.1 M HCl and hot deionized water until the pH of the solution became neutral. The samples were subsequently dried in an oven at 105 °C and stored. The produced activated carbon was designated as karanj fruit hull activated carbon or KFHAC.

2.3. Characterization of activated carbon

The Brunauer–Emmett–Teller (BET) surface area and micropore volume of KFHACs were determined under N_2 gas at −196 °C by using a physisorption analyzer (Micromeritics, Model ASAP 2020, USA). The scanning electron microscope (SEM) (Model Supra 35 VP, Germany) was used to observe the surface morphology of the samples, while a Fourier transform infrared (FTIR) spectrometer (Model 2000, Perkin–Elmer, USA) was used to verify the presence of surface functional groups before and after adsorption.

Table 1
Textural properties of KFHAC.

Single point surface area (m^2/g) at $P/P_0 = 0.2500$	849.66
BET surface area (m^2/g)	828.30
Langmuir surface area (m^2/g)	1145.84
External surface area (m^2/g)	84.86
BJH – cumulative pore volume (cm^3/g)	0.03
t-plot micropore volume (cm^3/g)	0.36
Average pore width (Angstrom, Å)	19.92

2.4. Batch adsorption experiments

Batch adsorption experiments were conducted in a 250 ml stopper Erlenmeyer flask with 0.20 g of KFHAC and 200 ml of MB solution at various concentrations (25, 50, 100, 200, 250, 300, 350 and 400 mg/l). The flasks were shaken at 120 rpm in a thermostatic water bath shaker at 30 °C. The adsorption process was optimized by varying the solution pH (3–13), contact time (0–28 h), initial dye concentration (25–400 mg/l), and solution temperature (30–50 °C). The pH of the dye solution was adjusted by adding 0.1 M HCl or NaOH. The desired pH was achieved through monitoring with a pH meter (EUTECH Instruments, Model Ecoscan, Singapore). The concentrations of MB were determined at different time intervals by using a double beam UV–vis spectrophotometer (Shimadzu, Model UV 1700, Japan) at 668 nm.

The adsorption capacity of MB at the equilibrium (q_e, mg/g) and removal percentage (R, %) were calculated using the following equations:

$$q_e = \frac{(C_o - C_e)V}{W} \quad (1)$$

$$R\% = \frac{(C_o - C_e)}{C_o} \times 100 \quad (2)$$

where C_0 is the initial MB concentration (mg/l), C_e is the concentration of MB at the equilibrium (mg/l), V is the volume of MB solution (l), and W is the mass of KFHAC (g).

For the point of zero charge (pH_{pzc}) determination the initial pH (pH_i) of aqueous solutions (100 ml) were adjusted to a pH range of 2–12 using 0.1/1.0 M HCl or NaOH. Then, 0.1 g of KFHAC was added to each adjusted solution. The dispersions were shaken for 48 h at 30 °C, and the final pH of the solutions (pH_f) was determined. The point of zero charge (pH_{pzc}) is the point where the curve pH_f vs. pH_i intersects the line $pH_f = pH_i$.

3. Results and discussion

3.1. Surface characteristics of KFHAC

Fig. 1 shows the N_2 adsorption–desorption isotherm at 77 K and the pore size distribution of KFHAC. Based on the International Union of Pure and Applied Chemistry classification, the N_2 adsorption–desorption isotherm belongs to the type I isotherm with a plateau parallel to the P/P_0 axis [27]. This observation indicates the microporous structure of KFHAC, with none or very low mesoporosity [16]. The textural parameters of KFHAC are summarized in Table 1. KFHAC presents an average pore size of approximately 19.92 Å, which indicates that the carbon consists of micropores (pore diameter < 20 Å) [27]. Furthermore, KFHAC shows BET surface area 828.30 m^2/g and micropore volume 0.36 cm^3/g which

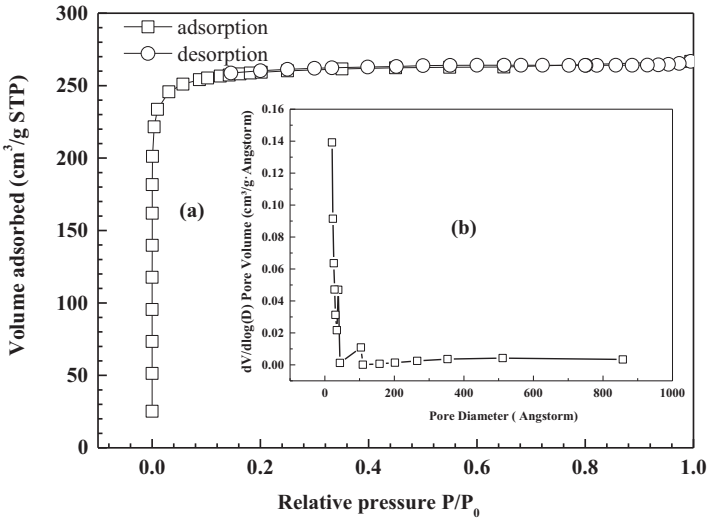

Fig. 1. (a) N_2-adsorption–desorption isotherm for KFHAC; (b) pore diameter and pore volume plot of KFHAC.

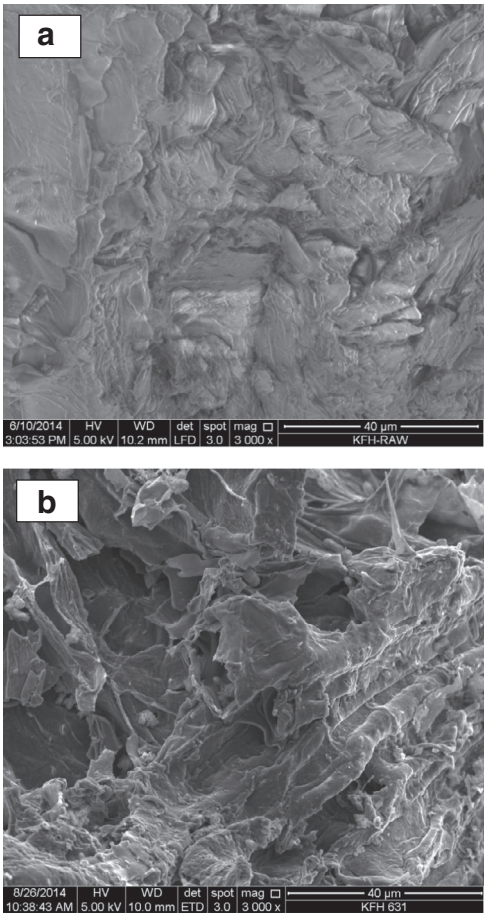

Fig. 2. SEM images of (a) KFH-R (3000×) and (b) KFHAC (3000×).

is analogous to those activated carbons obtained from KOH activation of other lignocellulosic materials such as cotton stalk which is reported to exhibit BET surface area 729.33 m^2/g and micropore pore volume 0.26 cm^3/g; and rambutan peel which exhibits BET surface area 971.54 m^2/g and micropore volume 0.16 cm^3/g [11, 17]. Therefore, karanj fruit hull is a promising precursor for the production of high-surface-area activated carbon.

Fig. 2 shows the SEM micrographs of KFH-R and KFHAC at 3000× magnification. The KFH-R surface is dense and planar and contains few pores, whereas the KFHAC surface presents a large surface area and enhanced porosity and contains pores with varied sizes and shapes. The KOH activator was responsible for the porosity development of the raw precursor by widening the existing pores and creating new pores. Therefore, MB cations can be trapped and adsorbed on the KFHAC surface.

FTIR analysis of KFHAC before and after MB adsorption was conducted to identify surface functional groups involved in binding to MB cations. Karanj fruit hulls consist high amounts of cellulose (11.73%), hemicellulose (47.28%), lignin (38.62%), and extractives (2.37%) [28]. However, most of these components would be eliminated during carbonization and activation, resulting in low and weak intensities of the absorption peaks for KFHAC (Fig. 3(a)). The band at 2981 cm^{-1} and its shoulder at 2885 cm^{-1} are attributed to νC–H and δC–H (ν= stretching and δ = bending) absorption bands, respectively, which indicates the presence of methyl and methylene groups in the precursor [11]. Other peaks at 1408, 1056, and 852 cm^{-1} are characteristics of the O–H bending of carboxylic acids, C–OH stretching vibration, and out-of-plane C–H bending vibration, respectively. After MB adsorption, some peaks disappeared and several functional groups shifted to different frequencies (Fig. 3(b)). There occurs the disappearance of peak at 3552 cm^{-1} and shifting of peak from 3537 to 3452 cm^{-1} which are attributed to O–H stretching vibrations and also disappearance of peak attributed to C=O stretching of carboxylic group at 1770 cm^{-1}. Therefore, O–H and C=O groups are the possible functional groups involved in the interaction between KFHAC and MB cations.

3.2. Adsorption studies

Fig. 4 shows the effect of initial dye concentration, which ranged from 25 mg/l to 400 mg/l, on MB removal by KFHAC. All the concentrations achieved the adsorption equilibrium within 24 h of contact time. Adsorption was initially fast because of the high driving force and rapid transfer of adsorbate ions to the surface of carbon particles. With increasing contact time, adsorption gradually slowed down before reaching the equilibrium state. Hence, the equilibrium state was achieved within a relatively long period because the dye molecules tend to diffuse into the porous KFHAC structure and utilize the active sites.

The pH_{pzc} is the pH where the adsorbent net surface charge corresponds to zero, and it offers the possible mechanism about the electrostatic interaction between adsorbent and adsorbate. The

Please cite this article as: Md.A. Islam et al., Nanoporous activated carbon prepared from karanj (*Pongamia pinnata*) fruit hulls for methylene blue adsorption, Journal of the Taiwan Institute of Chemical Engineers (2017), http://dx.doi.org/10.1016/j.jtice.2017.01.016

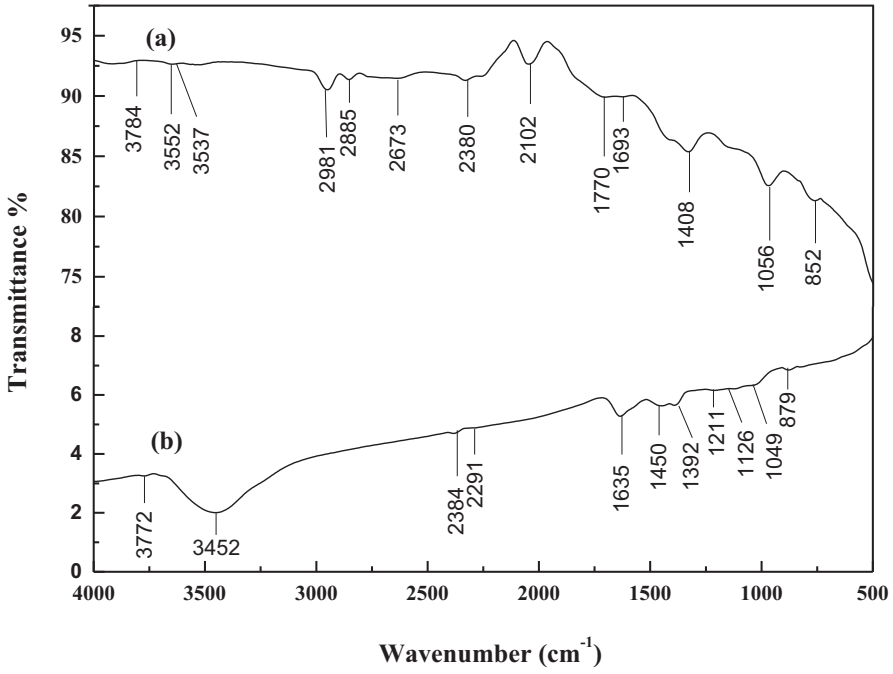

Fig. 3. FTIR spectra of KFHAC (a) before and (b) after MB adsorption.

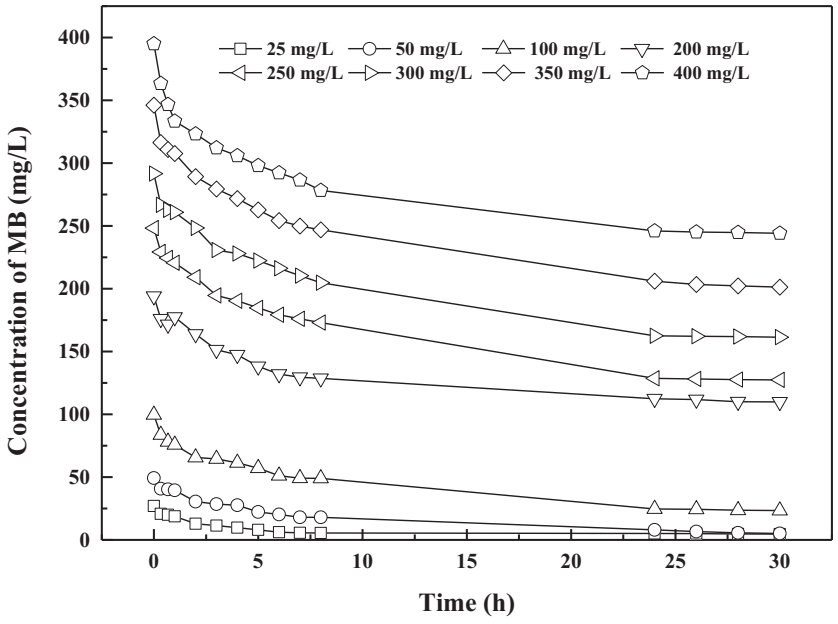

Fig. 4. Effect of initial dye concentrations on MB uptake by KFHAC at 30 °C.

pH_{pzc} value of 4.1 was obtained for KFHAC as shown in Fig. 5(a). Fig. 5(b) illustrates the effect of pH, which ranged from 3 to 13, on MB removal by KFHAC at an initial MB concentration of 100 mg/l. The surface of KFHAC is positively charged at the pH 4.41 and below. When the pH is increased (4–7), the MB uptake increases slightly as a consequence of the increase in electrostatic interactions between the cationic dye and KFHAC due to deprotonation of surface active sites. This means that there occurs decrease in the surface charge density of the adsorbent with increasing pH, thereby enhancing the electrostatic attractions between the positively charged MB cations and the negatively charged KFHAC surface.

$$MB^{+} + R - O^{-} \rightleftharpoons R - O^{-}{}^{+}MB \quad (3)$$

However, electrostatic driven adsorption process cannot explain the slight decrease in MB removal at pH 9–13. There might be another mode of adsorption like ion exchange or chelation which results in decrease of MB removal rates at higher pH [29].

3.3. Adsorption kinetics

In this work, kinetic study was performed to describe the rate and mechanism of adsorption. The kinetics of the adsorption process was interpreted using the non-linear pseudo-first- and

Please cite this article as: Md.A. Islam et al., Nanoporous activated carbon prepared from karanj (*Pongamia pinnata*) fruit hulls for methylene blue adsorption, Journal of the Taiwan Institute of Chemical Engineers (2017), http://dx.doi.org/10.1016/j.jtice.2017.01.016

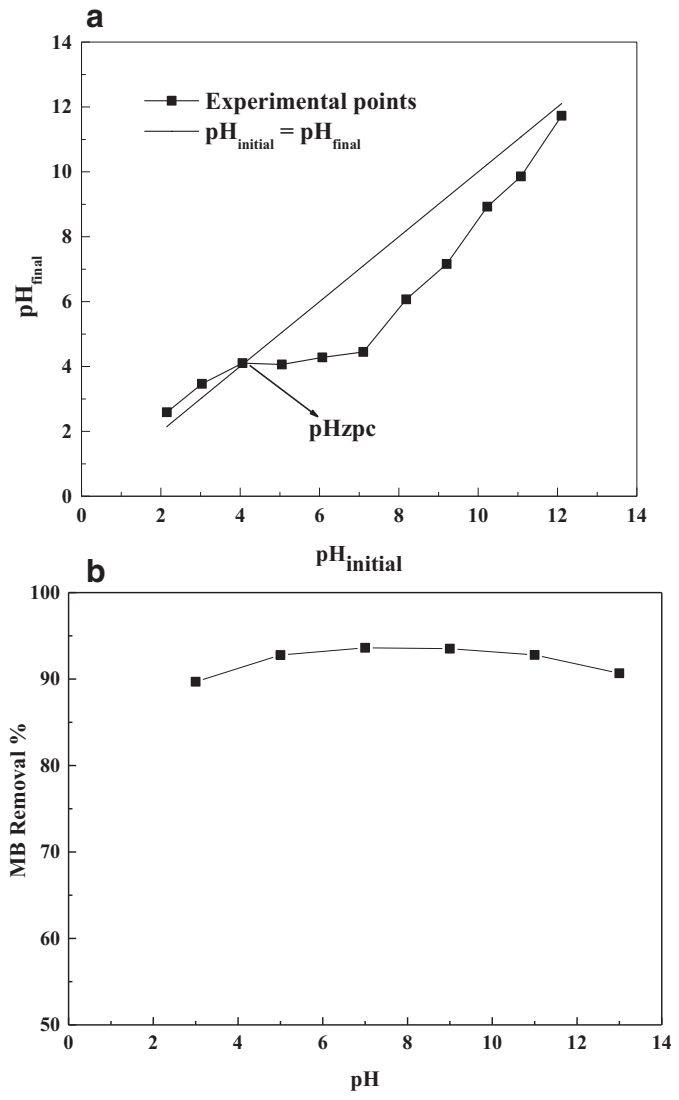

Fig. 5. (a) pH_{zpc} of KFHAC (b) effect of pH on MB removal by KFHAC at 30 °C.

pseudo-second-order kinetic models. The pseudo-first-order kinetic model was proposed by Lagergren and Svenska [30] and is given below:

$$q_t = q_e(1 - \exp^{-k1t}) \tag{4}$$

where q_e (mg/g) and q_t (mg/g) are the amounts of MB adsorbed on KFHAC at equilibrium and at time t, respectively; and k_1 (1/min) is the pseudo-first-order rate constant. The pseudo-second-order equation [31] is expressed as follows:

$$q_t = \frac{q_e^2 k_2 t}{1 + q_e k_2 t} \tag{5}$$

where k_2 (g/mg min) is the pseudo-second-order rate constant.

The best-fitted model was assessed using the coefficient of determination (R^2) and two non-linear error functions: normalized standard deviation (NSD) and average relative error (ARE). The equations of the functions are given as follows:

$$R^2 = 1 - \frac{\sum_{n=1}^{n} (q_{t.meas} - q_{t.cal})^2}{\sum_{n=1}^{n} (q_{t.cal} - \overline{q_{t.cal}})^2} \tag{6}$$

$$NSD = 100 \times \sqrt{\frac{1}{n-1} \sum_{i=1}^{n} \left[\frac{q_{t.meas} - q_{t.cal}}{q_{t.meas}} \right]^2} \tag{7}$$

$$ARE = \frac{100}{n} \sum_{i=1}^{n} \left[\frac{q_{t.meas} - q_{t.cal}}{q_{t.meas}} \right] \tag{8}$$

where $q_{t\cdot meas}$ (mg/g) and $q_{t.cal}$ (mg/g) are the experimental- and model-predicted adsorption capacity of MB at time t, respectively, and n is the number of observations. Low NSD and ARE values indicate accurate fitting of the model.

Fig. 6 shows the experimental kinetic data represented as q_t versus t for MB adsorption on KFHAC. The graph depicts that the equilibrium state was reached after 24 h of contact time, in which the rate of dye being adsorbed by the adsorbent is equal to the rate of dye being desorbed. At this point, dye concentration was constant in both phases. Furthermore, the adsorption capacities of MB on KFHAC rapidly increased from 21.9 mg/g to 149.9 mg/g as the initial dye concentration increased from 25 mg/l to 400 mg/l. The increase in capacity could be due to the collision between MB molecules and the KFHAC surface at high initial dye concentrations. Hence, large amounts of MB will be combined and adsorbed on KFHAC.

Fig. 6 also shows the predicted pseudo-first- and pseudo-second-order kinetic models for MB adsorption on KFHAC by using the non-linear method. The calculated values of the pseudo-first-order rate constant k_1, pseudo-second-order rate constant k_2, and predicted adsorption capacity $q_{t.mod}$ are given in Table 2. At high R^2 values, the NSD and ARE values were low in the pseudo-second-order kinetic model. Furthermore, the $q_{t.mod}$ values fitted well with the $q_{t\cdot exp}$ values. An accurate fit to the pseudo-second-order kinetic model suggests that chemisorption is the possible rate-determining step that controls the adsorption process; as such, the adsorption rate of MB is proportional to the number of active sites available on the KFHAC surface [32].

3.4. Adsorption isotherms

Adsorption isotherm is used to describe adsorbent–adsorbate interaction and the equilibrium distribution of adsorbate molecules at the solid–liquid phases [17]. The adsorption equilibrium was obtained by plotting the experimental amount of MB adsorbed, q_e (mg/g), against the dye concentration, C_e (mg/l), under equilibrium conditions (Fig. 7). The adsorption equilibrium was further evaluated using two isotherm models, namely, Langmuir and Freundlich.

The Langmuir isotherm model [33] describes the monolayer adsorption process on uniform adsorption sites and can be expressed as follows:

$$q_e = \frac{q_m K_a C_e}{1 + K_a C_e} \tag{9}$$

where K_a (l/mg) is the Langmuir constant and q_m (mg/g) is the maximum monolayer adsorption capacity.

The Freundlich isotherm model [34] describes the multilayer adsorption process on heterogeneous adsorption sites and can be expressed as:

$$q_e = K_f C_e^{1/n} \tag{10}$$

where K_f (mg/g (l/mg)$^{1/n}$) is the Freundlich constant that represents the adsorption capacity and n is the adsorption intensity.

Temkin isotherm deals with adsorbent–adsorbate interactions and their effect on linear decrease of heat of adsorption with coverage [35]. Its nonlinear form is expressed as:

$$q_e = B\ln(AC_e) \tag{11}$$

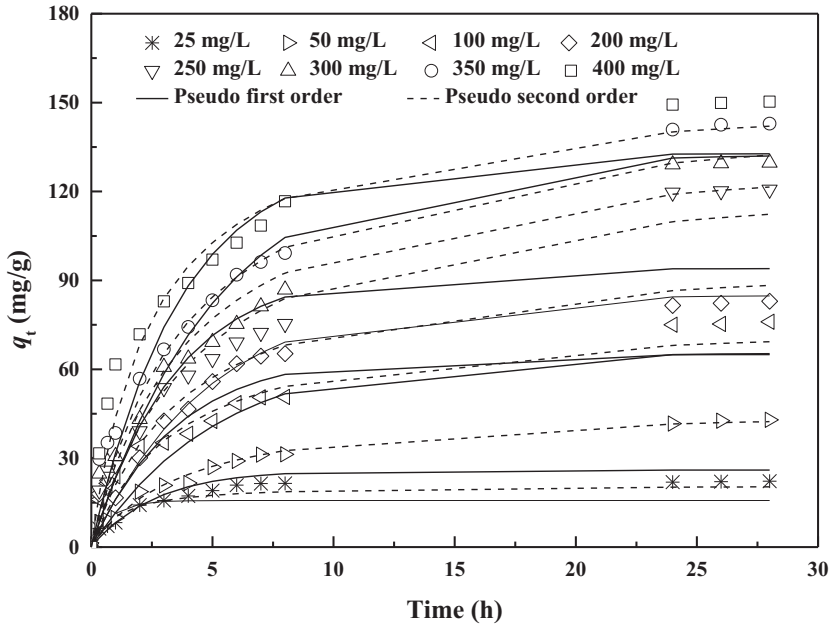

Fig. 6. Non-linear plots of the pseudo-first- and pseudo-second-order kinetic models for MB adsorption on KFHAC at 30 °C.

Table 2
Parameters of the pseudo-first- and pseudo-second-order kinetic models for MB adsorption on KFHAC at different initial dye concentrations.

Parameters	C_0 (mg/l)							
	25	50	100	200	250	300	350	400
$q_{e,\,exp}$ (mg/g)	22.1	42.6	75.3	82.85	120.15	129.5	142.7	149.9
Pseudo-first-order								
$q_{e,\,mod}$ (mg/g)	15.72	26.0	65.57	64.99	84.76	93.99	132.55	132.78
k_1(1/m)	0.021	0.006	0.003	0.004	0.003	0.004	0.003	0.004
R^2	0.4428	0.6173	0.6135	0.7689	0.6829	0.7088	0.7880	0.6135
NSD	55.37	157.80	121.63	100.88	110.51	83.61	83.14	73.39
ARE	48.61	91.29	50.04	65.44	90.28	50.35	29.89	37.24
Pseudo-second-order								
$q_{e,\,mod}$ (mg/g)	21.11	48.18	77.99	100.07	129.99	138.88	150.85	154.90
k_2(g/mg min)	0.0007	0.0001	0.0001	0.00004	0.00003	0.00003	0.00003	0.00004
R^2	0.9993	0.9769	0.9940	0.9668	0.9942	0.9895	0.9937	0.9899
NSD	40.44	100.74	90.70	47.62	67.62	60.81	68.92	54.10
ARE	19.31	5.06	19.53	2.41	6.52	5.67	21.25	13.65

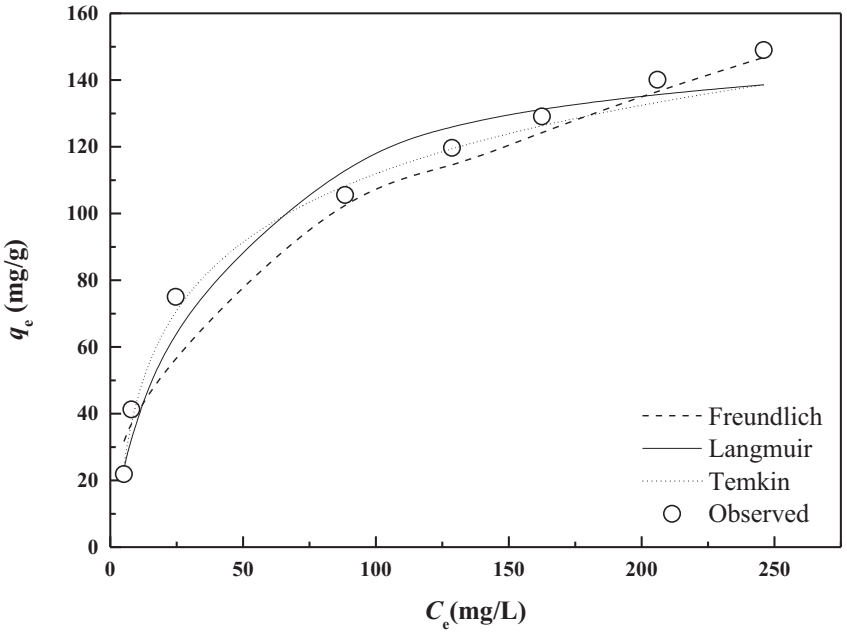

Fig. 7. Adsorption isotherm plots of the Langmuir, Freundlich and Temkin models for MB adsorption on KFHAC at 30 °C.

Please cite this article as: Md.A. Islam et al., Nanoporous activated carbon prepared from karanj (*Pongamia pinnata*) fruit hulls for methylene blue adsorption, Journal of the Taiwan Institute of Chemical Engineers (2017), http://dx.doi.org/10.1016/j.jtice.2017.01.016

Table 3
Parameters of the Langmuir, Freundlich and Temkin isotherm models for MB adsorption on KFHAC at different temperatures.

Model	Parameter	Temperature (°C)		
		30	40	50
Langmuir	q_m (mg/g)	154.8	203.4	239.4
	K_a (l/mg)	0.035	0.058	0.071
	R^2	0.9992	0.9976	0.9986
	RMSE	0.566	1.379	1.281
Freundlich	K_f (mg/g) (l/mg)$^{1/n}$)	19.16	36.44	43.21
	N	0.375	0.322	0.334
	R^2	0.9990	0.9961	0.9967
	RMSE	0.627	1.791	2.013
Temkin	A	0.44	0.37	0.53
	B	85.12	71.45	92.26
	R^2	0.9785	0.9673	0.9738
	RMSE	1.816	2.381	2.165

where $B=RT/b$ and corresponds to enthalpy of adsorption; b is Temkin constant related to heat of sorption (J/mol); and A is binding constant at equilibrium which corresponds to the maximum binding energy (l/g).

The best isotherm model was identified by the coefficient of determination (R^2) and validated using the residual root-mean squared error (RMSE), as shown below:

$$R^2 = 1 - \frac{\sum_{n=1}^{n} (q_{e.meas} - q_{e.cal})^2}{\sum_{n=1}^{n} (q_{e.meas} - \overline{q_{e.cal}})^2} \quad (12)$$

$$RMSE = \sqrt{\frac{1}{n-1} \sum_{n=1}^{n} (q_{e.meas} - q_{e.cal})^2} \quad (13)$$

where $q_{e.meas}$ (mg/g) and $q_{e.cal}$ (mg/g) are the experimental- and model-predicted adsorption capacity at equilibrium, respectively, and n is the number of observations.

Table 3 summarizes the calculated parameters of the three isotherm models. The Langmuir isotherm model, with higher R^2 and lower RMSE values, could better describe the adsorption process than the other two models. The results suggest that MB adsorption on KFHAC occurred on homogeneous sites, which are identical and contain equivalent energy. Furthermore, KFHAC exhibited relatively high adsorption capacities for MB. The calculated q_m was found to be 154.8, 203.4, and 239.4 mg/g at 30 °C, 40 °C, and 50 °C, respectively. The q_m of KFHAC was relatively high compared with other modified activated carbons for MB adsorption (Table 4). Therefore, karanj fruit hull is a viable precursor for the production of an effective and efficient activated carbon.

3.5. Adsorption mechanisms

MB adsorption on KFHAC may involve several steps including (a) film or external diffusion, (b) pore diffusion, (c) surface diffusion, and (d) adsorption on the pore surface. In this study, the pseudo-first- and second-order kinetic models could not determine the diffusion mechanism. Hence, the Weber–Morris intraparticle diffusion and Boyd models were used to clarify the adsorption mechanisms.

The Weber–Morris intraparticle diffusion model is based on Fick's second law of diffusion and given by the following formula [36]:

$$qt = k_{id} t^{1/2} + C \quad (14)$$

where k_{id} is the intraparticle diffusion rate constant (mg/g min$^{1/2}$) and C is the intercept related to the boundary layer effect (mg/g). The values of k_{id} and C can be obtained from the gradient and intercept of the linear plots of q_t versus $t^{1/2}$ (Fig. 8). The rate of pore diffusion and the intercept increased as the initial MB concentration increased from 25 mg/l to 400 mg/l (Fig. 8). This phenomenon could be due to the increase in the boundary layer thickness and driving force for adsorption associated with the initial dye concentration. The lines did not pass through the origin, thus implying that intraparticle diffusion is not the main diffusion mechanism.

The Boyd model [37] was employed to distinguish film and intraparticle diffusion. The linearized form of the model is generally expressed as follows:

$$\ln\left(1 - \frac{q_t}{q_e}\right) = -k_{fd} t \quad (15)$$

where k_{fd} is the liquid film diffusion constant determined from the gradient of the linear plots between $\ln(1-q_t/q_e)$ and t. The linear plot of the Boyd model did not pass through the origin (figure not shown). The R^2 values of the Boyd model were also higher than that of the intraparticle diffusion model (Table 5). Based on these findings, film diffusion is the rate-determining step that controls MB adsorption on KFHAC [38]. Similar adsorption mechanisms were reported by Njoku et al. [38] for carbofuran adsorption on activated carbon prepared from coconut frond.

3.6. Adsorption thermodynamics

Thermodynamic parameters, such as Gibbs free energy change ($\Delta G°$), enthalpy change ($\Delta H°$), and entropy change ($\Delta S°$), were calculated with the formulas below:

$$\ln K_d = \frac{\Delta S^\circ}{R} - \frac{\Delta H^\circ}{RT} \quad (16)$$

$$\Delta G^o = \Delta H^o - \Delta S^o T \quad (17)$$

Table 4
Assessment of the capacity of other activated carbons for MB adsorption.

Precursor	Bet surface area (m^2/g)	Activator	Activation temperature (°C)	Adsorption capacity (mg/g)	Reference
Albizia lebbeck seed pods	1824.88	KOH	Microwave-induced	381.22	[6]
Cotton stalk	729.33	KOH	Microwave-induced	294.12	[11]
Cotton stalk	621.47	K_2CO_3	Microwave-induced	285.71	[11]
Karanj fruit hul	828.30	KOH	600	239.40	Present study
Rambutan peel	971.54	KOH	Microwave-induced	215.05	[17]
Macadamia nut endocarp	598	$ZnCl_2$	Microwave-induced	194.70	[18]
Peach stone	1535	$ZnCl_2$	600	191.30	[19]
Coffee grounds	925	H_3PO_4	450	181.80	[20]
Posidonia oceanica fibres	946.55	H_3PO_4	600	137.27	[21]
Posidonia oceanica fibres	762.81	KOH	600	133.62	[21]
Posidonia oceanica fibres	502.88	$ZnCl_2$	600	114.89	[21]
Posidonia oceanica fibres	60.24	H_2O_2	600	600	[21]
Apricot stones	359.40	$H_3PO_4 + HNO_3$	700	36.68	[22]

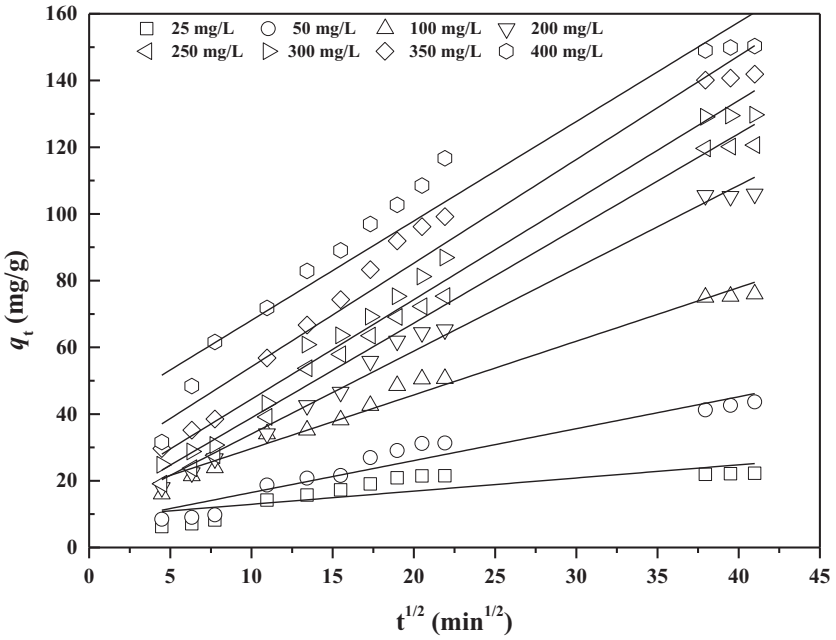

Fig. 8. Intraparticle diffusion model for MB adsorption on KFHAC.

Table 5
Parameters of the intraparticle and film diffusion models for MB adsorption on KFHAC at different initial dye concentrations.

Parameters	C_0 (mg/l)							
	25	50	100	200	250	300	350	400
Intraparticle diffusion model								
K_{id}	0.394	0.975	1.609	2.48	2.83	2.98	3.10	2.978
C	9.01	6.91	13.56	9.21	10.51	14.63	23.15	38.34
R^2	0.639	0.927	0.978	0.980	0.985	0.980	0.965	0.941
Film diffusion model								
K_{fd}	0.008	0.003	0.001	0.001	0.001	0.001	0.002	0.002
R^2	0.959	0.990	0.990	0.981	0.994	0.985	0.991	0.977

where K_d is the adsorption distribution constant (l/mg), R is the universal gas constant (8.314 J/mol K), and T is the absolute temperature (K).

The $\Delta G°$ values at 303 K, 313 K, and 323 K were determined as −0.269, −2.062, and −2.841 kJ/mol, respectively. The negative signs signifies the spontaneity of the adsorption process and energy generation during the process [38]. The decrease in the $\Delta G°$ values with temperature implies that MB adsorption on KFHAC is thermodynamically favorable at high temperatures. Furthermore, the positive value of $\Delta H°$ ($\Delta H° = 38.885$ kJ/mol) indicates the endothermic nature of the adsorption process, which is consistent with the findings in Section 3.4. The diffusion rate of MB molecules increased with increasing temperature. Hence, large amounts of MB will be adsorbed as numerous active sites were utilized across the external boundary layer and in the internal pores of KFHAC. The randomness or random distribution of sites covered by the adsorbate molecules at the solid–liquid interface also increased, as indicated by the positive sign of $\Delta S°$ ($\Delta S° = 0.130$ kJ/mol K).

4. Conclusion

This study explored the potential of karanj fruit hulls as a new and low-cost precursor of activated carbon. KFHAC presents a large surface area with a BET surface area of 828.30 m^2/g, a micropore volume of 0.36 cm^3/g, and an average pore size of 19.92 Å The adsorption experiments indicated that the adsorption kinetics could be best described by the pseudo-second-order kinetic model. Meanwhile, the Langmuir isotherm model best fitted the adsorption equilibrium data with the maximum adsorption capacities (q_m) of 154.8, 203.4, and 239.4 mg/g at 30 °C, 40 °C, and 50 °C, respectively. These results indicated that KFHAC is an efficient and effective adsorbent for MB adsorption.

Acknowledgments

The fourth author acknowledges the award of Universiti Sains Malaysia postdoctoral fellowship in aid for research. The authors appreciate the support of the Deanship of Scientific Research at the King Saud University for the Prolific Research Group PRG-1437-31.

References

[1] Hardin IR. Chemical treatment of textile dye effluent. In: Christie RM, editor. Environmental aspects of textile dyeing. Cambridge: Woodhead Publishing; 2007. p. 191–211.
[2] Marrakchi F, Khanday WA, Asif M, Hameed BH. Cross-linked chitosan/sepiolite composite for the adsorption of methylene blue and reactive orange 16. Int J Biol Macromol 2016;93:1231–9.
[3] Khanday WA, Asif M, Hameed BH. Cross-linked beads of activated oil palm ash zeolite/chitosan composite as a bio-adsorbent for the removal of methylene blue and acid blue 29 dyes. Int J Biol Macromol 2017;95:895–902.
[4] Haji A, Mousavi Shoushtari A, Abdouss M. Plasma activation and acrylic acid grafting on polypropylene nonwoven surface for the removal of cationic dye from aqueous media. Desalin Water Treat 2015;53:3632–40.
[5] Gao Y, Yue Q, Gao B, Sun Y, Wang W, Li Q, et al. Preparation of high surface area-activated carbon from lignin of papermaking black liquor by KOH activation for Ni(II) adsorption. Chem Eng J 2013;217:345–53.

[6] Ahmed MJ, Theydan SK. Optimization of microwave preparation conditions for activated carbon from *Albizia lebbeck* seed pods for methylene blue dye adsorption. J Anal Appl Pyrol 2014;105:199–208.
[7] Ahmad AA, Hameed BH, Ahmad AL. Removal of disperse dye from aqueous solution using waste-derived activated carbon: optimization study. J Hazard Mater 2009;170:612–19.
[8] Foo KY, Hameed BH. Utilization of rice husks as a feedstock for preparation of activated carbon by microwave induced KOH and K_2CO_3 activation. Bioresour Technol 2011;102:9814–17.
[9] Auta M, Hameed BH. Optimized waste tea activated carbon for adsorption of methylene blue and acid blue 29 dyes using response surface methodology. Chem Eng J 2011;175:233–43.
[10] Foo KY, Hameed BH. Microwave-assisted preparation and adsorption performance of activated carbon from biodiesel industry solid reside: influence of operational parameters. Bioresour Technol 2012;103:398–404.
[11] Deng H, Li G, Yang H, Tang J, Tang J. Preparation of activated carbons from cotton stalk by microwave assisted KOH and K_2CO_3 activation. Chem Eng J 2010;163:373–81.
[12] Chandra TC, Mirna MM, Sunarso J, Sudaryanto Y, Ismadji S. Activated carbon from durian shell: preparation and characterization. J Taiwan Inst Chem Eng 2009;40:457–62.
[13] Khanday WA, Marrakchi F, Asif M, Hameed BH. Mesoporous zeolite–activated carbon composite from oil palm ash as an effective adsorbent for methylene blue. J Taiwan Inst Chem Eng 2017;70:32–41.
[14] Noorimotlagh Z, Darvishi Cheshmeh Soltani R, Khataee AR, Shahriyar S, Nourmoradi H. Adsorption of a textile dye in aqueous phase using mesoporous activated carbon prepared from Iranian milk vetch. J Taiwan Inst Chem Eng 2014;45:1783–91.
[15] Haji A, Mahmoodi NM. Soy meal hull activated carbon: preparation, characterization and dye adsorption properties. Desalin Water Treat 2012;44:237–44.
[16] Ubago-Pérez R, Carrasco-Marín F, Fairén-Jiménez D, Moreno-Castilla C. Granular and monolithic activated carbons from KOH-activation of olive stones. Microporous Mesoporous Mater 2006;92:64–70.
[17] Njoku VO, Foo KY, Asif M, Hameed BH. Preparation of activated carbons from rambutan (*Nephelium lappaceum*) peel by microwave-induced KOH activation for acid yellow 17 dye adsorption. Chem Eng J 2014;250:198–204.
[18] Pezoti Junior O, Cazetta AL, Gomes RC, Barizão ÉO, Souza IPAF, Martins AC, et al. Synthesis of $ZnCl_2$-activated carbon from macadamia nut endocarp (*Macadamia integrifolia*) by microwave-assisted pyrolysis: optimization using RSM and methylene blue adsorption. J Anal Appl Pyrol 2014;105:166–76.
[19] Uysal T, Duman G, Onal Y, Yasa I, Yanik J. Production of activated carbon and fungicidal oil from peach stone by two-stage process. J Anal Appl Pyrol 2014;108:47–55.
[20] Reffas A, Bernardet V, David B, Reinert L, Lehocine MB, Dubois M, et al. Carbons prepared from coffee grounds by H_3PO_4 activation: characterization and adsorption of methylene blue and nylosan red N-2RBL. J Hazard Mater 2010;175:779–88.
[21] Ncibi MC, Ranguin R, Pintor MJ, Jeanne-Rose V, Sillanpää M, Gaspard S. Preparation and characterization of chemically activated carbons derived from Mediterranean *Posidonia oceanica* (L.) fibres. J Anal Appl Pyrol 2014;109:205–14.
[22] Djilani C, Zaghdoudi R, Djazi F, Bouchekima B, Lallam A, Modarressi A, et al. Adsorption of dyes on activated carbon prepared from apricot stones and commercial activated carbon. J Taiwan Inst Chem Eng 2015;53:112–21.
[23] Bora MM, Deka R, Ahmed N, Kakati DK. Karanja (*Millettia pinnata* (L.) Panigrahi) seed oil as a renewable raw material for the synthesis of alkyd resin. Ind Crop Prod 2014;61:106–14.
[24] Takase M, Zhao T, Zhang M, Chen Y, Liu H, Yang L, et al. An expatiate review of neem, jatropha, rubber and karanja as multipurpose non-edible biodiesel resources and comparison of their fuel, engine and emission properties. Renew Sustain Energy Rev 2015;43:495–520.
[25] Acharya SK, Swain RK, Mohanty MK. Emission analysis of using preheated karanja and kusum oil. Energy Source Part A 2014;36:1358–65.
[26] Salman JM, Njoku VO, Hameed BH. Batch and fixed-bed adsorption of 2,4-dichlorophenoxyacetic acid onto oil palm frond activated carbon. Chem Eng J 2011;174:33–40.
[27] Sing KSW, Everett DH, Haul RAW, Moscou L, Pierotti RA, Rouquérol J, et al. Reporting physisorption data for gas/solid systems with special reference to the determination of surface area and porosity. Pure Appl Chem 1985;57:603–19.
[28] Islam MA, Asif M, Hameed BH. Pyrolysis kinetics of raw and hydrothermally carbonized karanj (*Pongamia pinnata*) fruit hulls via thermogravimetric analysis. Bioresour Technol 2015;179:227–33.
[29] Hamdaoui O. Batch study of liquid-phase adsorption of methylene blue using cedar sawdust and crushed brick. J Hazard Mater 2006;135:264–73.
[30] Lagergren S. Zur theorie der sogenannten adsorption gelöster stoffe. K Sven Vetensk Handl 1898;24:1–39.
[31] Ho YS, McKay G. Sorption of dye from aqueous solution by peat. Chem Eng J 1998;70:115–24.
[32] Islam MA, Benhouria A, Asif M, Hameed BH. Methylene blue adsorption on factory-rejected tea activated carbon prepared by conjunction of hydrothermal carbonization and sodium hydroxide activation processes. J Taiwan Inst Chem Eng 2015;52:57–64.
[33] Langmuir I. The adsorption of gases on plane surfaces of glass, mica and platinum. J Am Chem Soc 1918;40:1361–403.
[34] Freundlich H. Über die adsorption in lösungen (adsorption in solution). Phys Z Chem 1906;57:384–470.
[35] Temkin MI, Pyzhev V. Kinetics of ammonia synthesis on promoted iron catalysts. Acta Physiochim URSS 1940;12:217–22.
[36] Weber WJ, Morris JC. Kinetics of adsorption on carbon solution. J Sanit Eng Div Proceed Am Soc Civ Eng 1963;89:31–59.
[37] Boyd GE, Adamson AW, Myers LS. The exchange adsorption of ions from aqueous solutions by organic zeolites. II. Kinetics. J Am Chem Soc 1947;69:2836–48.
[38] Njoku VO, Islam MA, Asif M, Hameed BH. Preparation of mesoporous activated carbon from coconut frond for the adsorption of carbofuran insecticide. J Anal Appl Pyrol 2014;110:172–80.

Please cite this article as: Md.A. Islam et al., Nanoporous activated carbon prepared from karanj (*Pongamia pinnata*) fruit hulls for methylene blue adsorption, Journal of the Taiwan Institute of Chemical Engineers (2017), http://dx.doi.org/10.1016/j.jtice.2017.01.016